Energy reduction by power loss minimisation through wheel torque allocation in electric vehicles: a simulation-based approach

(article starts on next page)

IA*VSD*

Taylor & Francis
Taylor & Francis Group

Energy reduction by power loss minimisation through wheel torque allocation in electric vehicles: a simulation-based approach

Juliette Torinsson[a,b], Mats Jonasson[b], Derong Yang[a] and Bengt Jacobson[b]

[a]Department of Vehicle Energy and Motion Control, Volvo Car Corporation, Göteborg, Sweden; [b]Department of Vehicle Engineering and Autonomous Systems, Chalmers University of Technology, Göteborg, Sweden

ABSTRACT

As vehicles become increasingly electrified, electrical machines for propulsion can be divided into many sources making the vehicle highly over-actuated. For over-actuated vehicles, the allocation of a propulsive force is an underdetermined process with respect to both the number of wheels and electrical machines. Hence, the allocation can be made to favour particular attributes such as energy consumption. In this study, a vehicle equipped with four identical electric motors with a fixed transmission ratio connected through a half-shaft and a coupling to one wheel respectively is driven a 2-h-long city cycle in the vicinity of Göteborg. Two different control allocation methods are presented to distribute torque momentaneously based on driver request while minimising power losses in electric motor and inverter as well as tyres. One method is a quadratic programming optimisation and the other is an offline exhaustive search method resulting in a look-up table based on requested torque and actual speed. The two methods are compared to other torque distribution strategies based on fixed distribution ratio and equal tyre-to-road friction utilisation. It was found that using the developed optimisation algorithms, a reduction of up to 3.9% in energy consumption can be obtained.

1. Introduction

The modern car industry is facing a great challenge to reduce emissions and thus environmental impact. Apart from the challenges connected to the production of electric vehicles, such as availability of battery metals and power grid network, user related issues such as long charging times and limited range impact the transition from fossil fuel to electricity as the primary energy source for freedom of movement. It is thus important to continuously improve energy efficiency of electric vehicles through all means possible.

Apart from afore-mentioned challenges, control related challenges are introduced with electric vehicles that have not before been present in petrol or diesel vehicles. An increased number of electric motors contribute to over-actuation in ground vehicles which was previously mainly seen in aircraft and marine vessels [1]. Over-actuation means that the motion

request from the driver can be attained in several different ways using different actuators. If a vehicle with four electric motors, one for each wheel, is driven and the electric motors could be used for both propulsion and regenerative braking, there is an infinite number of torque distributions that would fulfil the forward motion requested by the driver. If a steering request is added, even more solutions appear as yaw motion can be achieved either through propulsive or braking torques or steering of the wheels. The system of equations of motion is *underdetermined*, no unique solution exist. This underdetermined problem can be solved by control allocation.

One approach to solve the control allocation problem is by finding a solution through optimisation-based methods [2,3]. Using optimisation, a secondary objective can be added to the control allocation problem such as minimising wear of components or to minimise energy consumption. Various authors have investigated the possibility to reduce energy consumption in over-actuated electric vehicles through control allocation methods by finding the optimal torque distribution. A common approach is to solve the optimisation problem offline and create distribution rules which is then implemented in simulation or in a vehicle.

The authors in [4] use offline optimisation in the form of a quadratic program to find the optimal distribution between the motors based on a motor efficiency map. The optimal distribution is saved in a look-up table used online in simulation. In [5], offline optimisation is also used to find the optimal distribution between the motors based on a motor efficiency map. This is also the case in [6] and [7]. The authors in [8] have solved the problem using dynamic programming, also including the efficiency of the motors. Neither has included tyre losses in the cost function.

In [9], the control allocation problem is solved online through an active-set algorithm. The authors in [10] also solve the optimisation problem online. Online optimisation methods might however be harder to implement in a vehicle due to increased complexity compared to an analytical solution or distribution rules.

In [11,12] and [13], the control allocation problem is solved analytically and through offline optimisation respectively. The cost function consists of measured power losses at the wheel, including the electric motor drive, transmission and tyre. This approach is good in that the complexity of power loss functions of the complete drivetrain is avoided but includes a drawback that the measured experimental losses are very specific and hard to transfer to another vehicle with different types of electric motors and specifications.

Many of the distribution solutions above result in single axle operating at low torque demands, and both axles at high torque demands. In contrast to the above-mentioned work, the losses at zero torque of the electric motor, i.e. during the single axle torque distribution, have not yet been covered. The ability to decouple the motors and how to include a coupling in the optimisation process, as well as quantifying the energy savings potential in everyday driving is thus not yet well covered by the literature. Furthermore, the tyre losses are not included in many of the studies. In this study, the authors have investigated how to find the optimal torque distribution for longitudinal motion requests, with the possibility to decouple inactive motors, in order to minimise energy consumption and thus increase energy efficiency for the everyday driver. Two different optimisation based methods have been used to solve the control allocation problem and are compared to fixed distribution methods. The optimisation is done momentaneously, i.e. the optimal torque distribution that minimises the cost function is found in every time-step, as opposed to

predictive control. The optimisation of route and speed is assumed to be performed prior to the momentaneous optimisation of torque distribution by either a driver or driver function.

With this paper, the authors contribute to

- Introducing a coupling to avoid power loss from electric motors that rotate at zero torque and quantifying the additional energy saved
- Quantifying the reduction in energy consumption and categorise different power losses through a real-life city cycle corresponding to everyday driving
- Finding an energy efficient and real-time implementable torque distribution strategy by using offline optimisation
- Formulating the problem in a quadratic program and finding the analytical solution to the optimisation problem.

This paper is structured as follows. Section 2 presents the simulation environment including the vehicle model and drive cycle used. Section 3 describes the control architecture used to control the motor torques based on driver request. Section 4 describes the different power loss models that have been used in the objective function of the optimisation. Section 5 describes in detail the different control allocation methods and the fixed torque distribution strategies. Section 6 presents and discusses the results and Section 7 summarises the conclusions from this study.

2. Use-case description

The simulation environment is built in IPG CarMaker and Matlab Simulink. The control architecture described in Section 3 and the drivetrain including the battery, electric motors and gearbox are modelled in Simulink, and the vehicle dynamics of the chosen vehicle, the road as well as surrounding environment (aerodynamics, grade changes, etc.) is modelled in IPG CarMaker. The drivetrain model in Simulink exports wheel torque requests through external signals to the four wheels respectively in IPG CarMaker. The use case includes a driver-in-the-loop which is a default driver model in IPG CarMaker that follows a pre-defined path and velocity profile.

The vehicle used in this study is a passenger car with four identical permanent magnet synchronous machines (PMSM) connected to one wheel respectively through a coupling, fixed ratio transmission and a half-shaft. Each motor is directly controllable through torque requests and can be disconnected from the wheel by a controllable coupling. The maximum motor torque is 270 Nm from 0 to 4000 rpm, which then decreases as speed increases. This is seen in Figure 3. The shafts are assumed to be stiff, and the transmission ratio is fixed for each electric motor. The parameters for the vehicle and electric motor can be seen in Table 1.

A city cycle in the vicinity of Gothenburg (Sweden), Gothenburg City Cycle (GCC), will be used as a test cycle. The city cycle is approximately 66 km long and includes highway driving as well as driving in residential areas including many stops and speed breakers. It includes segments corresponding to normal driving, which makes it an appropriate test cycle for the purposes of this study. The cycle includes altitude data as well as speed restrictions. The g-g diagram of GCC can be seen in Figure 1(a). It shows the driving pattern of GCC in combination with selected driver model.

Table 1. Vehicle and tyre parameters.

Description	Symbol	Value
Total vehicle mass	m_{tot}	1988 kg
Front mass	m_{front}	1118 kg
Rear mass	m_{rear}	870 kg
Vehicle yaw inertia	I_{zz}	4300 kgm^2
Long. tyre stiffness front	$C_{f,x}$	235,000 N
Long. tyre stiffness rear	$C_{r,x}$	180,600 N
Unloaded tyre radius meas.	r_0	0.337425 m
Normal tyre load meas.	F_{z0}	4484 N
Tyre velocity meas.	v_{ref}	24.98 m/s^2
Tyre param. meas.	q_{sy1}	0.00890305
Tyre param. meas.	q_{sy2}	0.015
Tyre param. meas.	q_{sy3}	0.00654663
Tyre param. meas.	q_{sy4}	−0.000640923
Transmission ratio	n	10
Max motor torque (0 − 4000 rpm)	τ_{max}	270 Nm
Min motor torque (0 − 4000 rpm)	τ_{min}	−270 Nm
Max motor speed	ω_{max}	12000 rpm

(a) g-g diagram.
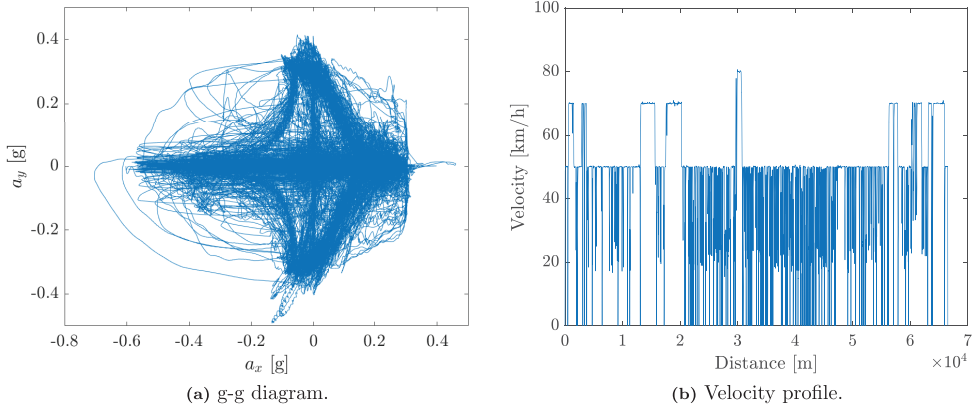
(b) Velocity profile.

Figure 1. Driving pattern of GCC: (a) g–g diagram and (b) velocity profile.

As can be seen, the deceleration levels are higher than the acceleration levels. The maximum lateral acceleration on either side is −0.4 g to 0.4 g, the maximum longitudinal acceleration and deceleration is 0.3 g and −0.6 g respectively. Hence, the driving pattern is not very aggressive and represents a moderate driver. The velocity profile presented in 1(b) shows that the speed is 50 km/h the majority of the distance with some short segments at 70 and 80 km/h. The use-case can then be summarised as moderate accelerations at medium driving velocities, suitable for the evaluation of everyday driving.

3. Control architecture

The vehicle used in this study is controlled by four identical PMSM. The study is limited to the longitudinal motion of the vehicle, i.e. yaw motion requests are not included. Reverse driving is not considered. The longitudinal dynamics control architecture can be seen in Figure 2.
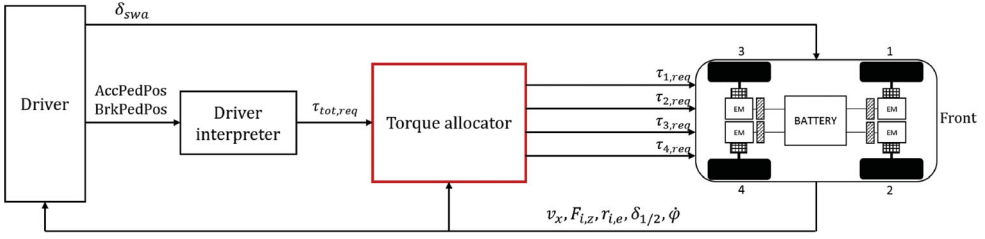
Figure 2. Vehicle longitudinal dynamics control architecture.
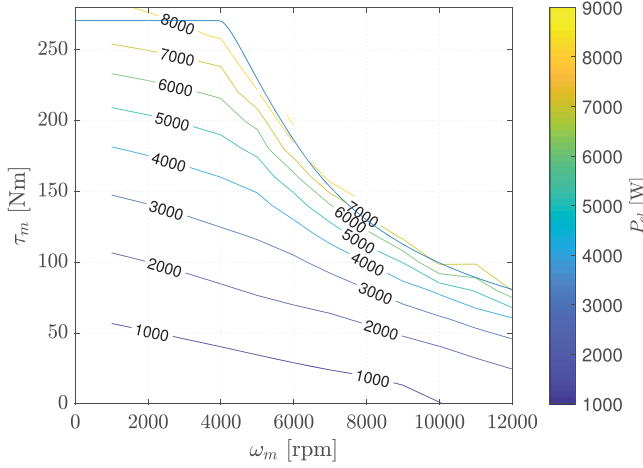
Figure 3. Test bench measured power loss data for a typical single electric motor and inverter pair.

The driver input consists of steering wheel angle (δ_{swa}), accelerator and brake pedal position (AccPedPos, BrkPedPos). The pedal positions are translated to a longitudinal force request ($F_{x,req}$) by being multiplied with a constant.

$$F_{x,req} = \gamma_1 \cdot \text{AccPedPos} - \gamma_2 \cdot \text{BrkPedPos} \tag{1}$$

where γ_1, γ_2 are constants. It is then converted to a total motor torque request through a conventional 'Driver interpreter' according to

$$\tau_{tot,req} = \frac{F_{x,req} \cdot r_l}{n} \tag{2}$$

where $\tau_{tot,req}$ is the requested total motor torque, r_l is the loaded radius averaged for all four wheels and n is the gear ratio. The wheels are numbered from 1 to 4 where 1 and 2 represent the front wheels, and 3 and 4 represent the rear wheels as indicated in Figure 2. The same numbering applies for the electric motors.

The torque is to be distributed in accordance with the active distribution strategy (described in Section 5) to the four electric motors in the 'Torque allocator' block. The requested total output torque is a hard constraint for the active distribution strategy.

4. Power loss models

The total energy consumption over a drive cycle can be approximated by the integral of work produced by the electric motors over the time it took to complete the cycle. If the optimisation of energy consumption is done momentaneously, it is not energy that is minimised but power losses in the system. Thus, in the remainder of this paper, losses refer to power losses unless stated otherwise.

The losses in a vehicle can be categorised into different groups, e.g. aerodynamic losses, tyre losses (rolling resistance and slip losses), transmission losses, electrical losses (motor, inverter, battery), etc. The aerodynamic losses are determined by hardware design such as shape of the vehicle profile, wheel houses, wheel rims, and under-body structure. They are included in the simulation environment but not considered in the torque allocation problem. Battery losses are dependent on resistance in the batteries and are variable with temperature, state of charge, current direction. They can however be modelled as an ohmic resistance multiplied with the current squared [14]. The battery losses are not considered in the optimisation, but with the same total torque input the battery losses are not expected to affect the distribution strategy found through control allocation. Assuming that the voltage is constant, the battery losses will vary with current which is dependent on total power consumed by the electric motors. Thus the battery losses can be expected to be less if the total power consumed by the electric motors is reduced. They do however affect the total energy consumption, and hence a lithium-ion battery model with round-trip efficiency of 95% is used according to [15]. The transmission losses are assumed to be linear with torque and will not affect the torque distribution, but the total energy consumption. The efficiency of the transmission is approximated to 97% also used in [15]. Since only the longitudinal dynamics is considered in this study, the lateral slip losses are not considered. The effect of combined slip is assumed negligible, since normal driving and high road friction are considered.

Remaining losses included and minimised in this study are: electric losses in the motor and inverter, longitudinal tyre slip losses and tyre rolling resistance losses. These are described in detail in the following section.

The electric losses are dependent on motor torque and speed. The tyre losses are modelled and depend on vertical tyre force, applied torque and translational and rotational wheel velocity.

4.1. Longitudinal slip loss

When applying a driving or braking torque to a wheel, longitudinal slip arises [16]. The slip results in a slip velocity that is defined as the difference between the translational velocity of the wheel centre and rotational velocity of the wheel multiplied with the effective wheel radius. The slip velocity gives rise to power loss characterised by the following formula [17]:

$$P_{s_x} = \sum_{i=1}^{4} F_{i,x}(\omega_i r_{i,e} - v_{i,x}) \tag{3}$$

where $F_{i,x}$ is the longitudinal force at the tyre contact patch, $r_{i,e}$ is the effective rolling radius of the freely rolling tyre, $v_{i,x}$ is the longitudinal velocity of the wheel centre and ω_i is the rotational wheel velocity of tyre i.

4.2. Rolling resistance loss

Rolling resistance arises due to the deflection of the carcass while rolling and hysteresis in the tyre [18]. As the tyre rotates, its rubber elements deflect upon coming into contact with the ground. The energy put into the deflection is not fully restored as the elements leave the contact patch due to internal damping in the tyre. This leads to a front-biased pressure distribution that gives rise to a moment in the opposite direction of the wheel rotation. The rolling resistance moment is defined as [16]

$$M_{i,y} = -F_{i,z} \cdot r_0 \cdot \left\{ q_{sy1} + q_{sy2} \cdot \frac{F_{i,x}}{F_{z0}} + q_{sy3} \cdot \left| \frac{v_{i,x}}{v_{ref}} \right| + q_{sy4} \cdot \left(\frac{v_{i,x}}{v_{ref}} \right)^4 \right\} \tag{4}$$

where $F_{i,z}$ is the vertical load of tyre i, r_0 is the unloaded tyre radius during the tyre measurement, $q_{sy1} - q_{sy4}$ are tyre fit parameters, F_{z0} is the vertical load during the tyre measurement, v_{ref} the translational velocity of the wheel centre during the tyre measurement.

The rolling resistance power loss for the four tyres can be expressed as

$$P_{RR} = \sum_{i=1}^{4} -M_{i,y} \cdot \omega_i \tag{5}$$

Rolling resistance is affected by a number of factors, e.g. structure of the tyre, operating conditions, normal load, tyre pressure and applied torque [18]. In Equation (4), the contribution of longitudinal force (indirectly applied torque) to rolling resistance moment is decided by the parameter q_{sy2}. In most tyre measurements, it is neglected and set to zero. Literature has investigated this contribution [19–21] and it can be found that for a passenger tyre, q_{sy2} take on the value of 0.015 for a bias belted tyre with 4000 N vertical load [19]. However, it is hard to know if this number is still relevant since passenger car tyres have been developed significantly since the study was conducted [22]. To the knowledge of the authors, there is no more recent study that has investigated this dependency, thus the value of 0.015 is used.

4.3. Electric losses

The electric losses from the electric motor and inverter are based on a loss map obtained in test bench experiments. They origin from iron and copper losses, and will increase non-linearly with torque and speed as seen in Figure 3. The experimental data is used directly in the offline optimisation scheme as described in Section 5.5.1. For the online optimisation described in Section 5.5.2, the losses are fitted with a polynomial of degree 2, according to Equation (6). The curve fit is displayed for three motor speeds in Figure 4. Here, the losses at zero torque, i.e. the losses when the motors rotate with the wheels but do not provide any torque, can be seen clearly. These losses are avoided by decoupling the motors from the wheels when the motors are not in use.
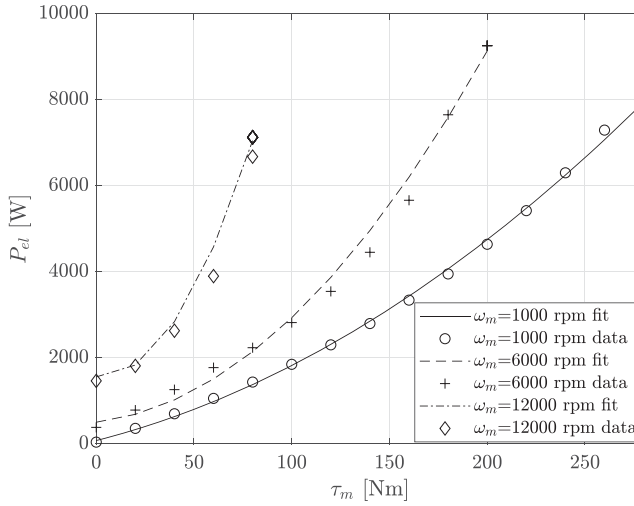
Figure 4. Quadratic curve fit of measured loss data for different motor rotational velocities.

The curve fit polynomial is expressed as

$$P_{el}(\boldsymbol{\tau_m}) = \sum_{i=1}^{4} p_2 \tau_{i,m}^2 + p_1 \tau_{i,m} + p_0 \tag{6}$$

where p_0, p_1 and p_2 are polynomial coefficients, $\boldsymbol{\tau_m}$ is the vector containing the motor torques $\tau_{i,m}$ for motor $i = 1,\ldots,4$. The polynomial is a function of motor torque and the coefficients vary with motor speed. The data is fitted separately for the positive and negative side of the torque spectrum. A quadratic curve fit is used due to the quadratic program formulated in Section 5 as a control allocation strategy. The motivation of using a quadratic program is also explained. A cubic curve fit would match the measured data points better, but the quadratic polynomial matches the data sufficiently well to support the usage of a quadratic program.

5. Torque distribution and allocation strategies

Six different torque distribution strategies are developed and compared in this study. A summary of the strategies can be seen in Table 2.

Three of them have a fixed torque distribution ratio between front and rear axle that will only change if the motors reach their max / min torque or tyres exceed their friction limit, and the other three are varying the torque distribution. The variation is done in accordance with two different goals depending on strategy; even friction utilisation of the wheels and minimising power losses. Concerning power loss minimisation, we consider two types of implementation methods using closed-loop numerical optimisation techniques. One is an on-board optimisation using a quadratic program where the optimal torque distribution is found at every time step. The other one is an offline optimisation resulting in a look-up table that provides the optimal torque distribution given the requested torque from the driver and current translational velocity of the vehicle. Since the study is limited to wheel

Table 2. Summary of torque distribution strategies.

Strategy	Description
FWD	Fixed distribution: two motors, front wheel drive. Rear motors are disconnected unless front motors are saturated
RWD	Fixed distribution: two motors, rear wheel drive. Front motors are disconnected unless rear motors are saturated
AWD ED	Fixed distribution: four motors, all wheel drive. Equal torque on all motors.
AWD EFU	Varying distribution: four motors, all wheel drive. Torque varies with normal load such that the tyre-to-road friction utilisation of each tyre is equal
Look-up	Varying distribution: look-up table for optimal torque distribution
QP	Varying distribution: quadratic program where the optimal torque distribution is found analytically

torque distribution for longitudinal motion requests, the requested yaw contribution from the motors is zero.

The different strategies will be applied for both propulsion and brake torques. It is most optimal to keep the motors on one side of the vehicle working in either traction or regeneration [13]. As an example, imagine the case where one axle is propelled while the other is being braked. One could view this scenario as the motor used for propulsion is charging the battery through the motor applying regenerative braking. Since there are both charging and discharging losses in the battery, more energy is consumed than if there where no regenerative braking. Thus no combination of positive and negative torque were investigated.

The torque is limited so that it does not exceed the maximum force, $F_{x,\max}$, that can be generated by tyres. The friction is assumed to be the same on each tyre. Since the torque is the limited to be the same axlewise, the force is limited by the smaller of the two according to

$$F_{j,x,\max} = a \cdot \min \left(\mu \cdot F_{j,z,right}, \mu \cdot F_{j,z,left} \right) \tag{7}$$

where j = front, rear and μ is the tyre-road friction coefficient which is assumed to be 1. The scalar a can be assigned any value in order to have a margin for stability or to cover uncertainties in tyre and road friction. The parameter should be tuned depending on Operational Driver Domain. In this study, the driver model represents a moderate driver and hence it is set to 0.8 which is close to 1. The maximum torque of an electric motor on a given axle is then defined as

$$\tau_{j,\max,F_x} = \frac{F_{j,x,\max} \cdot r_l}{n} \tag{8}$$

Furthermore, the torque is limited by the speed dependent minimum $\tau_{\min}(\omega_m)$ and maximum torque $\tau_{\max}(\omega_m)$ the electric motor can produce. The torque of a motor on the front or rear axle is thus limited by

$$\max(\tau_{j,\min,F_x}, \tau_{\min}(\omega_m)) \leq \tau_{j,\max} \leq \min(\tau_{j,\max,F_x}, \tau_{\max}(\omega_m)) \tag{9}$$

where j = front, rear, and ω_m is the speed of the motor. In case a torque limit is reached on one axle, the remaining requested torque is distributed to the motor pair on the other axle. The case where both axles reach their torque limit at the same time is not handled in this paper as it does not occur in the chosen test case.

5.1. Front wheel drive (FWD)

This strategy places all requested torque from the driver on the front axle. The rear motors are not connected unless needed if the front motors reach a torque limit.

$$\tau_1 = \tau_2 = \begin{cases} \frac{\tau_{tot,req}}{2} & \text{for } \frac{\tau_{tot,req}}{2} \leq \tau_{front,\max} \\ \tau_{front,\max} & \text{for } \frac{\tau_{tot,req}}{2} > \tau_{front,\max} \end{cases}$$

$$\tau_3 = \tau_4 = \begin{cases} 0 & \text{for } \frac{\tau_{tot,req}}{2} \leq \tau_{front,\max} \\ \frac{\tau_{tot,req}}{2} - \tau_{front,\max} & \text{for } \frac{\tau_{tot,req}}{2} > \tau_{front,\max} \end{cases}$$

5.2. Rear wheel drive (RWD)

This strategy places all requested torque from the driver on the rear axle. The front motors are not connected unless needed if the rear motors reach a torque limit.

$$\tau_1 = \tau_2 = \begin{cases} 0 & \text{for } \frac{\tau_{tot,req}}{2} \leq \tau_{rear,\max} \\ \frac{\tau_{tot,req}}{2} - \tau_{rear,\max} & \text{for } \frac{\tau_{tot,req}}{2} > \tau_{rear,\max} \end{cases}$$

$$\tau_3 = \tau_4 = \begin{cases} \frac{\tau_{tot,req}}{2} & \text{for } \frac{\tau_{tot,req}}{2} \leq \tau_{rear,\max} \\ \tau_{rear,\max} & \text{for } \frac{\tau_{tot,req}}{2} > \tau_{rear,\max} \end{cases}$$

5.3. All wheel drive, even distribution (AWD ED)

This strategy distributes the requested torque evenly between the four electric motors,

$$\tau_1 = \tau_2 = \tau_3 = \tau_4 = \frac{\tau_{tot,req}}{4} \tag{10}$$

5.4. Equal friction utilisation (AWD EFU)

This strategy makes use of the tyre-to-road friction, such that the utilisation of the tyre friction force is the same for each tyre. This means that the torque distribution is biased to axles with high normal load.

The relationship between the four tyres is determined by

$$\frac{F_{1,x}}{\mu F_{1,z}} = \frac{F_{1,x}}{\mu F_{1,z}} = \frac{F_{3,x}}{\mu F_{3,z}} = \frac{F_{4,x}}{\mu F_{4,z}} \tag{11}$$

where $F_{1,x}, \ldots, F_{4,x}$ are the longitudinal tyre forces of tyre 1,..., 4 as can also be seen in Figure 5, $F_{1,z}, \ldots, F_{4,z}$ are the vertical tyre forces and μ is the tyre-road friction coefficient.

The total longitudinal force request from the driver is expressed as a sum of the longitudinal tyre forces.

$$F_{x,req} = F_{1,x} \cos \delta_1 + F_{2,x} \cos \delta_2 + F_{3,x} + F_{4,x} \tag{12}$$

Adding the condition that the forces should be the same left and right one finds the following relationship:

$$F_x = 2 \left(F_{1,x} \cos \delta_1 + F_{3,x} \right), \quad F_x = 2 \left(F_{2,x} \cos \delta_2 + F_{4,x} \right) \tag{13}$$
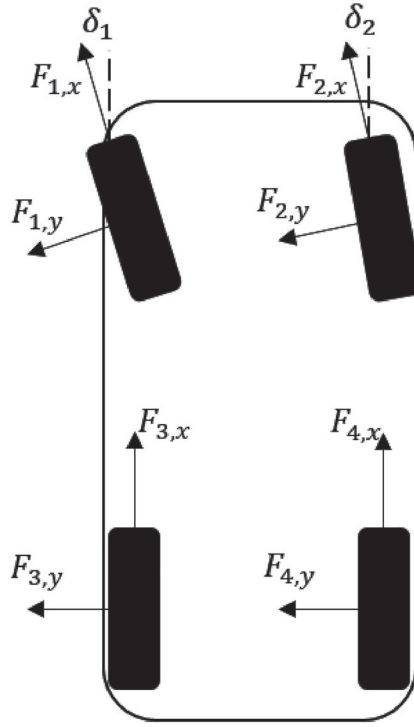
Figure 5. Vehicle model from a top view.

Rearranging Equations (11), (13), one finds expressions for the longitudinal forces. Translating them into motor torques for the four electric motors using Equation (2) results in the following expressions:

$$\tau_1 = \frac{\tau_{tot,req}}{2} \cdot \frac{F_{1,z}}{\left(F_{1,z}\cos\delta_1 + F_{3,z}\right)}, \quad \tau_2 = \frac{\tau_{tot,req}}{2} \cdot \frac{F_{2,z}}{\left(F_{2,z}\cos\delta_2 + F_{4,z}\right)} \tag{14}$$

$$\tau_3 = \frac{\tau_{tot,req}}{2} \cdot \frac{F_{3,z}}{\left(F_{1,z}\cos\delta_1 + F_{3,z}\right)}, \quad \tau_4 = \frac{\tau_{tot,req}}{2} \cdot \frac{F_{4,z}}{\left(F_{2,z}\cos\delta_2 + F_{4,z}\right)} \tag{15}$$

where $\tau_{tot,req}$ is the total motor torque requested by the driver. The vertical tyre forces $F_{i,z}$ and wheel steering angles δ_1, δ_2 are provided by CarMaker.

5.5. Control allocation strategies

Control allocation is an approach to solve the control problem concerning overactuated systems by distributing the total control demand among several actuators [2]. In control allocation, the actuator selection task is separated from the regulation task in the control design, making it well suited for systems with a large number and different types of actuators. Härkegård [2] defines a control allocator mathematically to solve 'an underdetermined, typically constrained, system of equations'. The input to the control allocator

is the requested control effect known as the virtual control input, $\mathbf{v(t)}$. The output of the control allocator are the requests to the actuators, $\mathbf{u(t)}$. Given $\mathbf{v(t)}$, $\mathbf{u(t)}$ is sought such that

$$\mathbf{v(t)} = \mathbf{g(u(t))} \tag{16}$$

where $\mathbf{g}$ is the mapping from the true control input to the virtual in the system to be controlled. Most commonly, a linear case is used where the relationship between virtual control input and the requests to the actuators is linearised. Linearising Equation (16) around $\mathbf{u_0}$ gives us

$$\mathbf{v(t)} = \mathbf{g(u_0)} + \mathbf{g'(u_0)} \cdot (\mathbf{u} - \mathbf{u_0}) \tag{17}$$

which can be rewritten as

$$\mathbf{v'(t)} = \mathbf{B} \cdot \mathbf{u(t)} \tag{18}$$

where

$$\mathbf{B} = \mathbf{g'(u_0)}, \quad \mathbf{v'(t)} = \mathbf{v(t)} - \mathbf{g(u_0)} + \mathbf{B} \cdot \mathbf{u_0} \tag{19}$$

$\mathbf{v'(t)} \in \mathbb{R}^{k\times1}$, $\mathbf{u(t)} \in \mathbb{R}^{m\times1}$, $\mathbf{B} \in \mathbb{R}^{k\times m}$ where $\mathbf{B}$ is called the control effectiveness matrix with rank $m > k$, meaning that there are no unique solutions to the system of equations (18).

In this paper, we reserve the term 'control allocation' for allocation where the secondary objective is momentaneous minimisation of power losses. Two control allocation methods are developed and presented here. The first uses an exhaustive search method offline that generates an electric drive mode map used on-board. The second method uses online quadratic programming to minimise power losses in real time.

The cost function is defined as a summation of the power consumption from the electric motors, including the electric losses and the tyre losses, according to,

$$P_{loss} = P_{el} + P_{RR} + P_{s_x} \tag{20}$$

where P_{el} is the electrical power losses of the motors and inverters, P_{RR} is the power losses due to rolling resistance, and P_{s_x} is the power losses due to longitudinal tyre slip.

The optimisation problem then becomes

$$\min_{\boldsymbol{\tau_m}} P_{loss} \tag{21}$$

such that
$$\begin{cases} \tau_{tot,req} = \sum_{i=1}^{4} \tau_{i,m} \\ 0 = \frac{w \cdot n}{2 \cdot r_l} \left(-\tau_{1,m} + \tau_{2,m} - \tau_{3,m} + \tau_{4,m} \right) \end{cases} \tag{22}$$

where the vector $\boldsymbol{\tau_m}$ containing the motor torques $\tau_{i,m}$ is the optimisation variable and w is the track width of the vehicle. The second constraint is the yaw contribution from the motors which is set to zero in this study. The speed dependent torque limits are not incorporated in the optimisation problem due to the desire to keep the simplicity. They are limited afterwards.

5.5.1. Offline optimisation: exhaustive search method (look-up table)

The exhaustive search method results in a look-up table that is used in the simulation environment. An operating range is defined for the electric motors dependent on total motor torque request from the driver and different motor velocities.

$$\tau_{tot,req} \in [-270, 270] \text{ Nm}, \quad \omega_m \in [0, 12000] \text{ rpm}$$

The torque requests and velocities are combined to create a map of operating points. For each operating point, all possible torque combinations fulfilling the desired motion request is found according to the linear system of Equation (23). This includes all combinations when motors are coupled and decoupled individually.

$$\mathbf{v} = \mathbf{B} \cdot \mathbf{u} \tag{23}$$

$$\mathbf{v} = \begin{bmatrix} \tau_{tot,req} \\ 0 \end{bmatrix}, \quad \mathbf{B} = \begin{bmatrix} 1 & 1 & 1 & 1 \\ -\dfrac{w \cdot n}{2 \cdot r_l} & \dfrac{w \cdot n}{2 \cdot r_l} & -\dfrac{w \cdot n}{2 \cdot r_l} & \dfrac{w \cdot n}{2 \cdot r_l} \end{bmatrix}, \quad \mathbf{u} = \begin{bmatrix} \tau_{1,m} \\ \tau_{2,m} \\ \tau_{3,m} \\ \tau_{4,m} \end{bmatrix} \tag{24}$$

The value of the cost function, i.e. the total power losses, is found for every remaining solution. Both longitudinal slip and rolling resistance loss will vary with load transfer during driving which are due to, e.g. longitudinal and lateral accelerations and road grade. In order to keep the number of dimensions low, the load transfer is not considered and the static normal loads are used. The optimal torque distribution providing the lowest power loss is then found for every operating point defined by the operating range of total torque request and motor velocity. The map of operating points is extended by a third dimension of torque distribution modes providing the lowest power losses for all individual operating points.

It was seen that the majority of optimal torque distributions were limited to three distribution modes. Thus, in order to simplify the table, there are only three possible torque distributions; equal torque on the front motors ($\tau_1 = \tau_2$, $\tau_3 = \tau_4 = 0$), rear motors ($\tau_1 = \tau_2 = 0$, $\tau_3 = \tau_4$) or all four motors ($\tau_1 = \tau_2 = \tau_3 = \tau_4$). When only two motors are in use, the other two motors will be decoupled in order to avoid power losses at zero torque. The optimal torque distribution mode is represented by an index (1, 2 or 3) which is saved in a table where one axis is total motor request based on the driver demand and the second axis is motor speed, resulting in a look-up table. Figure 6 visualises how the look-up table is used in simulation. A total torque request and current motor rotational velocity is provided as input to the look-up table, an algorithm finds the corresponding optimal torque distribution at given operating point, and the driving or braking torques are distributed accordingly.

5.5.2. On-board optimisation: quadratic programming (QP)

This is an on-board, closed-loop optimal controller where the analytic solution to a quadratic program (QP) of the cost function is found real-time in simulation. By using a quadratic formulation, there will always be a global minimum present due to the convex property of the optimisation problem given a convex set-up of constraints. Using problem formulations of higher order might increase the computation time and poses a risk of
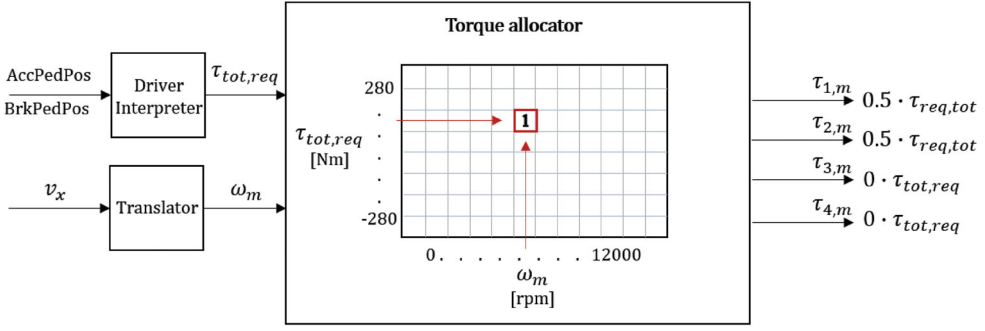
Figure 6. How the look-up table is implemented in vehicle verification.

finding sub-optimal solutions due to local minima. The optimisation problem with convex constraints is defined in the following way:

$$\min_{\mathbf{x}} \left(\frac{1}{2}\mathbf{x}^T \mathbf{Q}\mathbf{x} + \mathbf{f}^T\mathbf{x} \right)$$

such that $\mathbf{E} \cdot \mathbf{x} = \mathbf{d}$,

$$\text{where } \mathbf{x} = \boldsymbol{\tau_m} = \begin{bmatrix} \tau_{1,m} \\ \tau_{2,m} \\ \tau_{3,m} \\ \tau_{4,m} \end{bmatrix}, \quad \mathbf{d} = \begin{bmatrix} \tau_{tot,req} \\ 0 \end{bmatrix} \tag{25}$$

where $\mathbf{Q}$ contains the coefficients related to the second degree term in the quadratic function, $\mathbf{f}$ contains the coefficients to the first degree term, $\mathbf{E}$ is the matrix defining the relationship between the optimisation variable $\mathbf{x}$ and requests $\mathbf{d}$. The optimisation problem (25) can be relaxed by introducing a Lagrange multiplier λ and including the equality constraints in the objective function.

$$\min_{\boldsymbol{\tau_m},\lambda} \left(\frac{1}{2}\boldsymbol{\tau_m}^T \mathbf{Q}\boldsymbol{\tau_m} + \mathbf{f}^T\boldsymbol{\tau_m} + \lambda \left(\mathbf{E}\boldsymbol{\tau_m} - \mathbf{d} \right) \right) \tag{26}$$

The optimisation problem is now unconstrained and can be solved analytically through

$$\begin{bmatrix} \boldsymbol{\tau}_{m,opt} \\ \lambda \end{bmatrix} = \begin{bmatrix} \mathbf{Q} & \mathbf{E}^T \\ \mathbf{E} & \mathbf{0} \end{bmatrix}^{-1} \begin{bmatrix} -\mathbf{f} \\ \mathbf{d} \end{bmatrix} \tag{27}$$

Now, the expressions for power losses ((3), (5) and (6)) to be minimised need to be rearranged as quadratic functions of motor torque $\boldsymbol{\tau_m}$ in order to fit into the quadratic format (25).

By using a linear tyre model (28), the definition of longitudinal slip (29) and the conversion from longitudinal force to motor torque (2), one can rewrite the longitudinal slip power loss function (3) to (30). A linear tyre model is sufficient here since the city cycle use case in this paper reaches a maximum of approximately 4% slip, while the maximum force is usually reached between 15–20% slip [18]. Thus we can assume that the tyres will

work in the linear region.

$$F_{i,x} = C_{j,x} \cdot s_{i,x} \tag{28}$$

$$s_{i,x} = \frac{\omega_i r_{i,e} - v_{i,x}}{v_{i,x}} \tag{29}$$

$$P_{s_x} = \sum_{i=1}^{4} \frac{v_{i,x} \cdot n^2}{C_{j,x} \cdot r_l^2} \cdot \tau_{i,m}^2 \tag{30}$$

where $C_{j,x}$ is the longitudinal tyre slip stiffness of axle j and $s_{i,x}$ is the longitudinal tyre slip for tyre $i = 1,\dots,4$.

The rolling resistance moment (4) can be rearranged resulting in the following power loss expression:

$$P_{RR} = \sum_{i=1}^{4} \frac{F_{i,z} r_0 q_{sy2} \omega_i}{r_{i,e} F_{z0}} \tau_{i,m} \cdot n + F_{i,z} r_0 \omega_i \left(q_{sy1} + q_{sy3} \left| \frac{v_{i,x}}{v_{ref}} \right| + q_{sy4} \left(\frac{v_{i,x}}{v_{ref}} \right)^4 \right) \tag{31}$$

As can be seen, there is a constant term in (31) that is not dependent on $\tau_{i,m}$. This term will not affect the optimal torque distribution but will affect the total power loss.

The electric power losses (6) are already formulated as a quadratic function of $\boldsymbol{\tau_m}$ and can simply be added to the matrices $\mathbf{Q}$ and $\mathbf{f}$. However, this formulation also has a constant term corresponding to electric power losses at zero torque. These losses cannot be included in the optimisation since they are not dependent on $\boldsymbol{\tau_m}$, but can be avoided by decoupling the motors.

In order to include the presence of a coupling, three quadratic programs are formulated for three different motor utilisation strategies. One regards all four electric motors as coupled, one regards only the front motors as coupled and the rear motors as disconnected through the coupling, and one regards the rear motors as coupled and the front motors as disconnected through the coupling. The three quadratic programs are to symbolise AWD, FWD and RWD respectively. The optimisation formulation for the three programs are identical apart from the FWD and RWD having two additional equality constraints stating that the torque on either rear or front axle should be zero.

The motor losses, longitudinal wheel slip and rolling resistance losses are combined in the quadratic program formulation (25) according to

$$\mathbf{Q} = \text{diag} \left(p_2 + \left(\frac{v_{1,x} \cdot n^2}{C_{f,x} r_{i,e}^2} \right), p_2 + \left(\frac{v_{2,x} \cdot n^2}{C_{f,x} r_{2,e}^2} \right), p_2 + \left(\frac{v_{3,x} \cdot n^2}{C_{r,x} r_{3,e}^2} \right), p_2 + \left(\frac{v_{4,x} \cdot n^2}{C_{r,x} r_{4,e}^2} \right) \right)$$

$$\mathbf{f} = \begin{bmatrix} p_1 + n \cdot \omega_1 \cdot \left(q_{sy2} \dfrac{F_{1,z} r_0}{r_{1,e} F_{z0}} \right) \\[2ex] p_1 + n \cdot \omega_2 \cdot \left(q_{sy2} \dfrac{F_{2,z} r_0}{r_{2,e} F_{z0}} \right) \\[2ex] p_1 + n \cdot \omega_3 \cdot \left(q_{sy2} \dfrac{F_{3,z} r_0}{r_{3,e} F_{z0}} \right) \\[2ex] p_1 + n \cdot \omega_4 \cdot \left(q_{sy2} \dfrac{F_{4,z} r_0}{r_{4,e} F_{z0}} \right) \end{bmatrix}$$

The constant term of the rolling resistance power loss and electric power loss are defined below

$$k_{RR} = \sum_{i=1}^{4} \left(F_{i,z} r_0 \left(q_{sy1} + q_{sy3} \left| \frac{v_{i,x}}{v_{ref}} \right| + q_{sy4} \left(\frac{v_{i,x}}{v_{ref}} \right)^4 \right) \right) \tag{32}$$

$$k_{AWD} = 4 \cdot p_0 \quad k_{FWD} = k_{RWD} = 2 \cdot p_0 \tag{33}$$

where p_0, p_1 and p_2 are the coefficients of the motor loss polynomial, see Equation (6). The variables $v_{i,x}$, $r_{i,e}$, ω_i and $F_{i,z}$ are provided by CarMaker.

Furthermore, the optimisation algorithm is divided into two parts: one for positive and one for negative $\tau_{tot,req}$. This is due to different quadratic curve fit polynomials for positive and negative torques, since the curve fit for the entire torque spectrum was ill-matched. This will limit the resulting torque solutions to the same sign on each active motor, i.e. both motors must work in either traction or regeneration.

The matrix $\mathbf{E}$ and vector $\mathbf{d}$ for the QP representing the AWD case are defined below.

$$\mathbf{E_{AWD}} = \begin{bmatrix} 1 & 1 & 1 & 1 \\ -\dfrac{w \cdot n}{2 \cdot r_l} & \dfrac{w \cdot n}{2 \cdot r_l} & -\dfrac{w \cdot n}{2 \cdot r_l} & \dfrac{w \cdot n}{2 \cdot r_l} \end{bmatrix} \quad \mathbf{d_{AWD}} = \begin{bmatrix} \tau_{tot,req} \\ 0 \end{bmatrix} \tag{34}$$

Apart from meeting the motion requests, the two QPs where only one axle is coupled have the following additional equality constraints:

$$\tau_{1,m} = \tau_{2,m} = 0 \quad \text{or} \quad \tau_{3,m} = \tau_{4,m} = 0 \tag{35}$$

The solutions then become unique and are given by (36).

$$\mathbf{u_{FWD}} = \begin{bmatrix} \dfrac{\tau_{tot,req}}{2} \\ \dfrac{\tau_{tot,req}}{2} \\ 0 \\ 0 \end{bmatrix} \quad \mathbf{u_{RWD}} = \begin{bmatrix} 0 \\ 0 \\ \dfrac{\tau_{tot,req}}{2} \\ \dfrac{\tau_{tot,req}}{2} \end{bmatrix} \tag{36}$$

The final power loss of the three QPs are calculated according to

$$P_{loss,j} = \frac{1}{2} \boldsymbol{\tau_{m,opt,j}}^T \mathbf{Q} \boldsymbol{\tau_{m,opt,j}} + \mathbf{f}^T \boldsymbol{\tau_{m,opt,j}} + k_{RR} + k_j \tag{37}$$

where j = AWD, FWD or RWD. The optimisation problems are solved in parallel analytically through (27) and the optimal solution is then given by the QP providing the smallest power losses. The complete on-board optimisation problem can then be seen as a hybrid problem where the optimal solution is found by a combination of algorithms.
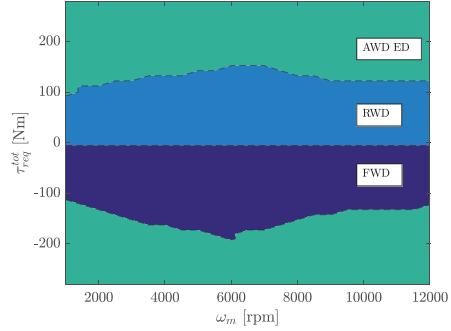
$$\boldsymbol{\tau_{m,opt}} \sim \min \left(P_{loss,AWD}, P_{loss,FWD}, P_{loss,RWD} \right) \tag{38}$$
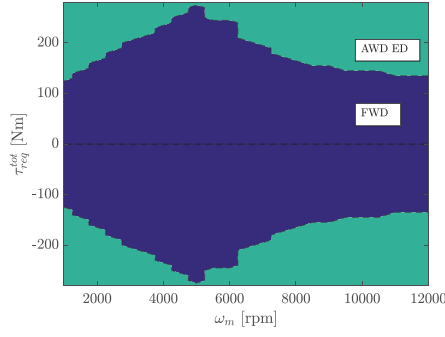
(a) Operational modes, based on only electric losses in the cost function.
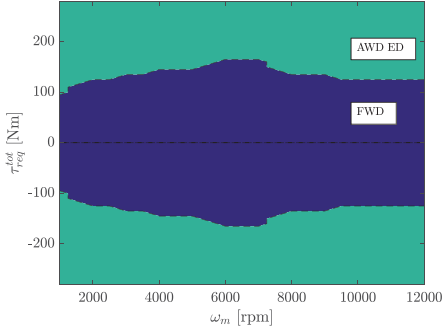
(b) Operational modes, based on electric losses longitudinal wheel slip losses in the cost function.

(c) Operational modes, based on electric losses longitudinal wheel slip losses and rolling resistance losses in the cost function.

Figure 7. Look-up table resulting from offline optimisation. Dark blue represents FWD, light blue represents RWD and green represents AWD ED: (a) operational modes, based on only electric losses in the cost function; (b) operational modes, based on electric losses longitudinal wheel slip losses in the cost function; (c) operational modes, based on electric losses longitudinal wheel slip losses and rolling resistance losses in the cost function.

6. Results

In this section, the results from the torque distribution and allocation methods are presented and compared. Initially, the optimal torque distributions resulting from the control allocation strategies will be presented; the look-up table resulting from the exhaustive search method and a comparison between the two strategies in order to see fundamental differences. Then, the power losses and the energy consumption will be presented.

6.1. Optimal torque distribution

The look-up table that results from the offline optimisation can be seen in Figure 7. On the vertical axis is the total torque requested to fulfil motion request from the driver, on the horizontal axis is the current motor (vehicle) speed, and the coloured areas in the figure symbolises either FWD, RWD or AWD ED.

The three different losses, electric, slip and rolling resistance, are added in steps to see how they each affect the distribution individually. Figure 7(a) represents the distribution when the cost function only includes the electric losses from the motor and inverter. At

(a) With coupling.　(b) Without coupling.
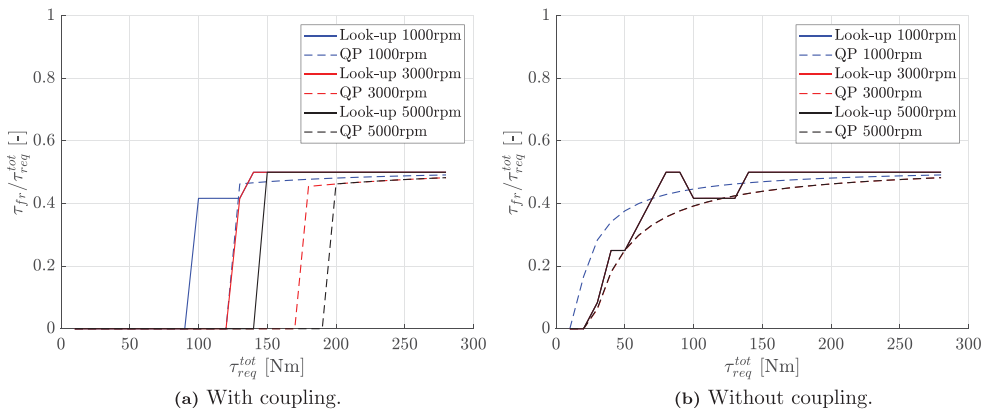
Figure 8. Front to total torque distribution ratio for three different motor speeds, comparison between offline optimisation and QP: (a) with coupling and (b) without coupling.

lower torque requests, on both sides of the torque spectrum (positive and negative), it is more energy efficient to use two motors. As the total torque request increases past a certain limit, it is more energy efficient to use four motors. At this point, it does not matter whether the front or rear motors are used for lower torque requests as the motors are identical.

Figure 7(b) shows the distribution when longitudinal slip is added to the cost function. The torque limit for where the distribution switches are lowered as high torque is penalised by high slip losses. Furthermore, now it makes a difference whether to use the front or rear motors in the two motor distribution. Since the vehicle has higher normal load on the front wheels, the slip losses are smaller for the same force generation compared to the rear axle, and thus it is more energy efficient to use FWD.

In the final step, Figure 7(c), rolling resistance loss is added. This is the final look-up table used in simulation. The addition of rolling resistance loss changes the torque distribution strategy for propulsion from FWD to RWD. The rolling resistance power losses favour axles with lower normal load, which is in conflict with the slip loss. The torque limit for switching distribution remains approximately the same. One can clearly see from the three figures that depending on which losses are included in the cost function, the optimal torque distributions will be different. Load transfer is not included in the offline optimisation, but the vehicle has a weight distribution biased towards the front axle. Thus the static normal load is higher in the front than the rear which is reflected in the look-up table.

In Figure 8, the effect of using quadratic polynomials to approximate electric losses in motor and inverter can be seen. The optimal torque distribution for the offline optimisation (exhaustive search method) and QP are compared in Figure 8(a) and 8(b), with and without coupling respectively. The curve fit of the electric losses makes the optimal torque distribution change to four motors at higher torques compared to the offline optimisation. The torque limit to change to four motors is pushed towards higher torque requests as the speed increases. Removing the coupling, it is still most optimal to use the rear motors for low torque requests, and change to four motors when the torque request increases. The torque limit however is much lower when all motors are connected at all times.

Furthermore, it can also be seen that there is a transition period between two motors and four motors where the torque distribution is not equal on all four motors. As mentioned
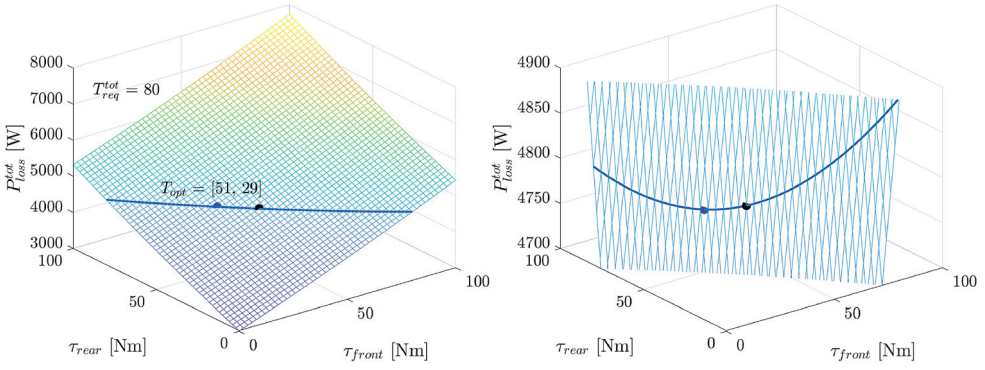
Figure 9. Illustration of the power minimisation strategy for $\tau_{tot,req} = 80$ Nm. The line represents all wheel torque distribution solutions between front and rear axles fulfilling $\tau_{tot,req} = 80$ Nm. The black dot corresponds to equal wheel torque on front and rear axles, $\tau_{front} = \tau_{rear} = 40$ Nm, and the blue dot corresponds to the optimal torque distribution where $\tau_{rear} = 51$ Nm and $\tau_{front} = 29$ Nm.

before, this transition is disregarded in a later stage to simplify the look-up table so that the AWD distribution only includes equal torque on all four motors. Here, we consider the transition control at actuator level so that a smooth mode change can be achieved.

Due to the convexity of the quadratic program, one might assume that the optimal distribution using four motors would be to divide the total torque request equally. However, this is not always the case. The total power losses as a function of front and rear axle torque can be seen in Figure 9. Here, it is clear that even though the cost function is in the form of a quadratic program, the optimal solution is not equal distribution on all four motors. This is a result of the tyre losses not being equal on the two axles, and thus the quadratic functions for the two axles are not equal. The line in the leftmost graph of Figure 9 represents a total torque request of 80 Nm, and the front and rear axle combinations satisfying this request. The magnified area clearly shows that the optimal solution is a torque distribution more biased towards the rear axle as opposed to the black dot which represents an equal distribution.

A rapid transition in torque distribution from RWD to AWD can be seen in Figure 10.

Both the optimal torque solutions through the look-up table and QP will start by propelling the rear wheels only. As the torque request is high enough around 0.3 s, they will change to four motors. Then, at around 5 s, the torque distribution will switch back to propelling the rear motors. In the lower graph of Figure 10, representing the power losses, a comparison between the two control allocation methods and two fixed torque distribution strategies can be seen; RWD and AWD ED. The two control allocation methods will follow the strategy that provides the least amount of power losses. At around 0.3 s, power losses for the RWD distribution will exceed the losses for AWD ED, and thus the control allocation strategies change torque distribution. Once more, at approximately 5 s, the power losses for AWD ED are now higher than for RWD, and thus another rapid transition in torque distribution occurs. This can be predicted by Figure 7(c) where the optimal strategy was shown as RWD at relatively low torque request.

The total energy losses for the different driving strategies can be seen in Figure 11.
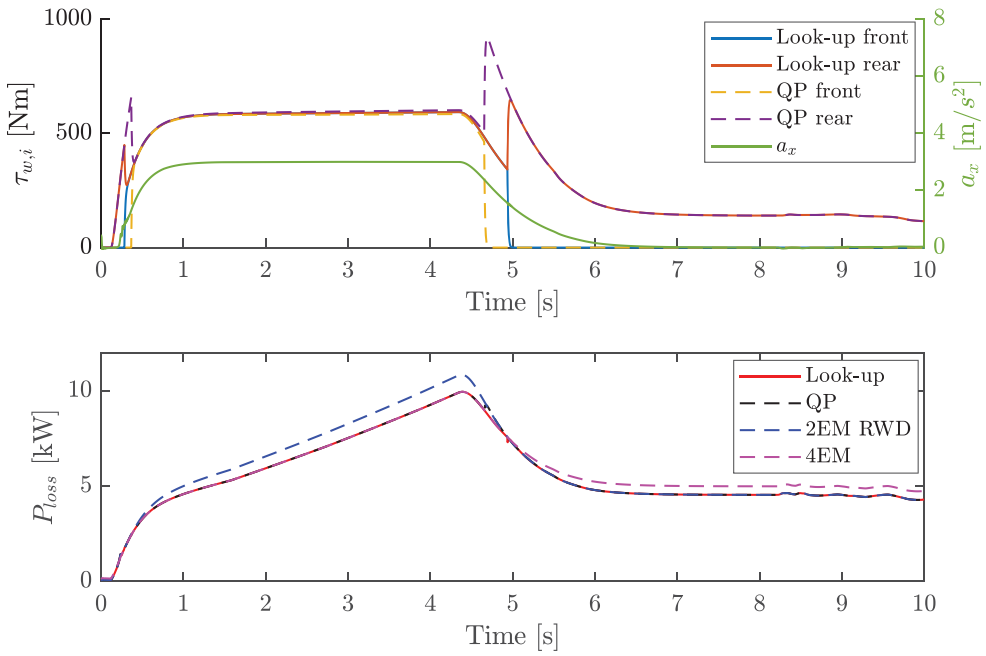
Figure 10. Time segment showing a switch in wheel torque distribution.
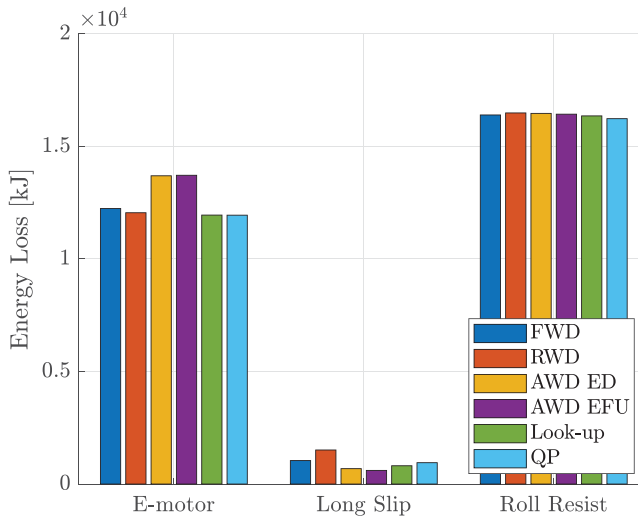
Figure 11. Energy losses for the different strategies.

Comparing the two motor strategies FWD and RWD with AWD ED, the electric energy losses are smaller using only two motors. The strategy with lowest electric losses is RWD, which is an effect of the torque limited by the available friction force described in Section 5.2. Since the rear axle has the lowest normal load, the friction force limit is reached at lower braking torques compared to the front axle. Thus in braking conditions, four motors are used more often in the RWD strategy compared to FWD. The driver brakes

Table 3. Energy consumption GCC.

Strategy	[MJ]	Savings
FWD	43.0	2.7%
RWD	43.4	1.8%
AWD ED	44.2	ref
AWD EFU	44.1	0.2%
Look-up	42.4	3.9%
QP	42.4	3.9%
QP w/o coupling	44.1	0.2%

harder than he accelerates (see Figure 1a), i.e. with higher torque, which according to Figure 7(c) favours a four-motor mode. Look-up and QP have the lowest electric losses overall.

Moving on to longitudinal slip losses, the strategy with the smallest losses is AWD EFU. By distributing the torque between four wheels, the torque on each wheel will be lower leading to smaller slip losses. The AWD EFU strategy maintains the same dynamic friction coefficient on all four wheels, which leads to that the torque distribution will be biased towards the axle with higher normal load. The slip losses will reduce further in this case since slip is higher for the axle with lower normal load compared to the heavier axle for the same applied torque. Regarding the two control allocation strategies, look-up performs better than QP. This is likely due to information about electric power losses that is lost in the quadratic curve-fitting. The strategy with the highest longitudinal slip losses is RWD, which can be expected due to the lower normal load on the rear axle. The rolling resistance losses are similar for all strategies, with QP once more providing the lowest values closely followed by look-up.

The energy consumption for the different strategies can be seen in Table 3. The strategy that consumes the least amount of energy is look-up, followed by QP. The small difference between these two justify the use of a second degree polynomial of the curve fit of electric losses in the motor and inverter. Compared to AWD ED, the optimisation strategies, i.e. Look-up and QP, are 3.9% more energy efficient. The coupling makes it possible to avoid the losses at zero torque, seen in Figure 4. By removing the coupling, thus keeping the motors connected at all times, the improvement by using QP compared to AWD ED is approximately 0.2%. Hence it can be concluded that a substantial part of the total losses origin from drag losses of the electric motors. Introducing a coupling increases the reduction in energy consumption by 3.7%-units. The difference between the strategies will greatly depend on which driving cycle and the driving pattern of the driver. GCC includes many segments of relatively flat, straight line driving at constant speed, where the torque demand is low. Thus it would be most beneficial to propel two motors only and decouple the remaining two according to Figure 7. This is also seen in Table 3 since the FWD and RWD strategies have lower energy consumption than AWD ED.

The validity of the rolling resistance coefficient q_{sy2} can be discussed as a lot of development of tyres have taken place since study in the paper providing this value was conducted. Even though rolling resistance in general has decreased over the years, it is hard to say if the relationship between applied torque and rolling resistance has changed or not. This study however suggests that there is energy to be saved by taking this dependence into account. It might not seem much, but every fraction of a percentage in less energy consumed is worth investigating.

7. Conclusion

This paper investigates different strategies for momentaneous control allocation including a controllable coupling, with respect to how they affect energy consumption through complete vehicle simulation using IPG CarMaker and Matlab Simulink. The strategies are designed so that they fulfil the motion request exactly, and use the over-actuation for other purposes such as power loss minimisation.

Two control allocation strategies, offline and online, are compared to three fixed distribution strategies and an equal friction utilisation strategy. Offline exhaustive search method generated a look-up table where three fixed torque distributions were defined; two motors FWD, two motors RWD or four motors AWD with equal distribution. It was found that at low torque demands, it is more energy efficient to distribute the torque on two motors while disconnecting the inactive motors through the coupling. During acceleration and low total torque demand, the axle with lowest normal load should be used and during deceleration with low total torque demand, the axle with highest normal load should be used. Independent of acceleration or deceleration, at higher torque demands it is most efficient to allocate torque equally to all four motors. It was found that by using this look-up table, a reduction of up to 3.9% in energy consumption was reached compared to equal torque distribution on all four wheels.

The cost function was also formulated in the form of a quadratic program where the optimal torque distribution to minimise the cost was found analytically. By using onboard optimisation in the form of a quadratic program as a control allocation strategy, the energy consumption decreased by 3.9% compared to AWD ED. It was also shown that a majority of the energy reduction, 3.7%, origins from the ability to decouple the motors, thus avoiding losses at zero torque. The solutions from the quadratic program provide torque distributions more biased towards the axle with lower normal load and adapts to variations in normal load. This strategy is, however, more complicated to use in-vehicle as it requires real time estimation of normal loads.

Comfort and stability during rapid change in torque on the four motors have not been investigated. Oscillations due to transient motor dynamics will affect the drivability of the vehicle and must be assessed before implementing in a real vehicle. Rapid changes of torque during a turn might cause stability issues and unexpected behaviour of the vehicle which is not wanted. The city cycle used in this study has significant longitudinal and lateral accelerations but quite low velocities, meaning that no stability issues were revealed during the rapid torque transitions. Further studies on more aggressive or low-mu scenarios must be performed in order to assess the safety criteria for the torque transitions. The energy efficient algorithm developed must then be incorporated with existing stability functions in the vehicle which have been neglected here.

Regarding implementation in a real vehicle, the look-up table is recommended as it only needs the actual vehicle speed and torque request from the driver. However, when yaw motion is taken into account, it will become significantly more complex as a third dimension is added. Thus the look-up table is suitable for longitudinal force request, but not necessarily for yaw moment request.

In conclusion, it has been shown that through a simple and implementable control allocation strategy, everyday driving can be made more energy efficient through control based on driver requests on longitudinal motion. Future studies will include yaw motion adding

steering angle as a control input, additional tyre losses, battery losses and stability as well as comfort analysis.

Acknowledgments

Disclosure statement

No potential conflict of interest was reported by the author(s).

Funding

References

[1] Chen Y, Wang J. Energy-efficient control allocation with applications on planar motion control of electric ground vehicles. In Proceedings of American Control Conference; 2011.

[2] Härkegård O. Backstepping and control allocation with applications to flight control. Linköping Studies and Science and Technology, Dissertations No. 820, 2003.

[3] Johansen TA, Fossen TI. Control allocation – a survey. Automatica. 2013;49:1087–1103.

[4] Pennycott A, De Novellis L, Sorniotti A, et al. The application of control and wheel torque allocation techniques to driving modes for fully electric vehicles. SAE Int J Passeng Cars – Mech Syst. 2014;7(2):

[5] Zhang X, Göhlich D. Optimal torque distribution strategy for a four motorized wheels electric vehicle international electric vehicle symposium and exhibition, EVS28; May 2015.

[6] Fujimoto H, Harada S. Model-based range extension control system for electric vehicles with front and rear driving-Braking force distributions. IEEE Trans Indust Electronics. May 2015;62(5):3245–3254.

[7] Pennycott A, De Novellis L, Sabbatini A, et al. Reducing the motor power losses of a four-wheel drive fully electric vehicle via wheel torque allocation. Proceedings of the Institution of Mechanical Engineers Part D Journal of Automobile Engineering; June 2014.

[8] Wu X, Zheng D, Wang TTorque optimal allocation strategy of all-Wheel drive electric vehicle based on difference of efficiency characteristics between axis motors. Energies. March 2019.12:1122.

[9] Chen Y, Wang J. Energy-efficient control allocation for over-actuated systems with electric vehicle applications. Proceedings of the ASME 2010 Dynamic Systems and Control Conference; September 2010.

[10] Chen Y, Wang J. Adaptive energy-efficient control allocation for planar motion control of over-actuated electric ground vehicles. IEEE Trans Control Syst Technol. July 2014;22(4

[11] Dizqah AM, Lenzo B, Sorniotti A, et al. A fast and parametric torque distribution strategy for four-wheel-drive energy-Efficient electric vehicles. IEEE Trans Indust Electron. July 2016;63(7):4367–4376.

[12] De Filippis G, Lenzo B, Sorniotti A, et al. Energy-efficient torque-vectoring control of electric vehicles with multiple drivetrains. IEEE Trans Vehicular Technol. June 2018;67(64702–4715.

[13] Lenzo B, De Filippis G, Sorniotti A, et al. Torque distribution strategies for energy-efficient electric vehicles with multiple drivetrains. J Dyn Syst Meas Control. Dec. 2017;1391

[14] Onori S, Serrao L, Rizzoni G. Hybrid electric vehicles. London: Springer; 2016. (Springer Briefs in Electrical and Computer Engineering).

[15] Genikomsakis KN, Mitrentsis G. A computationally efficient simulation model for estimating energy consumption of electric vehicles in the context of route planning applications. Transportation Res Part D. 2017;50:98–118.

[16] Pacejka H. Tire and vehicle dynamics. Oxford: Elsevier Science & Technology; 2012.
[17] Sina N, Esfahanian V, Hairi Yazdi MR, et al. Introducing the modified tire power loss and resistant force regarding longitudinal slip. SAE Int J Passeng Cars – Mech Syst. 2018;11(2):167–176.
[18] Wong JY. Theory of ground vehicles. 4th ed. John Wiley & Sons; 2008.
[19] Schuring DJ, Bird KD, Martin JF. Power requirements of tires and fuel economy. Tire Sci Technol, TSTCA. Nov. 1974;2(4):261–285.
[20] Roberts GB. Power wastage in tires. Proceedings, International Rubber Conference; Washington, DC: American Chemical Society; 1959, p. 57–72.
[21] Schuring DJ. Energy loss of pneumatic tires under freely rolling, braking and driving conditions. Tire Sci Technol, TSTCA. Feb. 1976;4(1):3–15.
[22] Nokian Tyres. Reducing the rolling resistance. [cited 2019 Dec 2]; Available from: https://www.nokiantyres.com/company/sustainability/products/reducing-the-rolling-resistance/.